



ELSEVIER

Available online at www.sciencedirect.com

SCIENCE @ DIRECT®

Combustion and Flame 141 (2005) 360–370

**Combustion
and Flame**www.elsevier.com/locate/combustflame

Experimental investigation of silane combustion and particle nucleation using a rapid-compression facility

M.T. Donovan¹, X. He, B. Zigler, T.R. Palmer, S.M. Walton,
M.S. Wooldridge*

Department of Mechanical Engineering, University of Michigan, 2350 Hayward Street, Ann Arbor, MI 48109-2125, USA

Received 29 April 2004; received in revised form 1 December 2004; accepted 31 January 2005

Available online 3 March 2005

Abstract

Ignition and reaction kinetics of silane/oxygen/diluent ($\text{SiH}_4/\text{O}_2/\text{Ar}/\text{N}_2$) mixtures have been studied using a rapid compression facility (RCF). Time-resolved pressure profiles and absolute, quantitative hydroxyl radical mole fraction (χ_{OH}) time histories were obtained for a range of conditions representing different heating rates. At the moderate temperatures studied (~ 630 K), ignition was observed to occur in two stages with no OH detected during the first stage. The separation of the two stages was typically >5 ms, thus the long test times provided by the RCF were critical to the studies. The second stage of reaction is identified by significant production of OH ($\chi_{\text{OH}} = 45\text{--}82$ ppm). Experimental uncertainty in χ_{OH} was $32/\text{--}29\%$ with a 15 ppm detectivity limit. The results were examined in the context of proposed silane combustion and particle nucleation reaction mechanisms. Existing silane combustion kinetics mechanisms capture many of the experimentally observed features of the system, yet fail to quantitatively reproduce the OH time histories in their entirety.

© 2005 The Combustion Institute. Published by Elsevier Inc. All rights reserved.

Keywords: Silane; Combustion; Hydroxyl radical; Absorption spectroscopy; Rapid-compression facility; Particle nucleation

1. Introduction

Understanding silane (SiH_4) combustion reaction kinetics is important for advances in combustion synthesis systems (where silane is used as a silica (SiO_2) nanoparticle precursor [1–3], in hydrogen (H_2) ignition applications (where silane has been proposed as a means to extend H_2 ignition limits [4,5]), and

for safety [6] and contamination considerations [7] (where silane is used in low-temperature anaerobic environments for wafer fabrication). For example, reaction kinetics have been proposed as critical to the early stages of SiO_2 particle nucleation. Self-clustering of SiO and SiO_2 monomers and addition of SiH_2O and HSiOOH to these clusters were suggested by Suh et al. [8] as key steps in the nucleation of SiO_2 nanoparticles at low-pressure, moderate temperature conditions.

There are few quantitative data on silane combustion. Silane ignition has been studied at high temperatures using shock tubes [4,9], and silane explosions have been studied at low temperatures [10 and references therein, 11]. Of these studies, there are no ab-

* Corresponding author. Fax: (734)-647-3170.

E-mail address: mwool@umich.edu

(M.S. Wooldridge).

¹ Current address: National Institute of Standards and Technology, USA.

solute, quantitative time-resolved species data available for validation of reaction mechanisms, although Peterson and Crofton [9] do provide normalized excited hydroxyl radical (OH^*) data. Based on this critical need, the objective of the current work was to provide improved understanding of both silane ignition and particle nucleation chemistry via rapid compression facility (RCF) experiments of silane mixtures. Absolute, quantitative OH time histories were obtained in the experiments as a means to validate the role OH plays in chain-branching radical production and in nucleation chemistry via H/Si/O clustering kinetics. The University of Michigan (UM) RCF is an ideal facility for these studies as long test times (> 10 ms) are required to study the processes of ignition and particle nucleation.

2. Experimental approach

A fixed frequency UV absorption diagnostic is used to measure the concentration of the hydroxyl radical, and the UM-RCF is used to generate the elevated temperature conditions characteristic of ignition and particle nucleation in the silicon/oxygen system. A detailed description of the UM-RCF, the operating procedures, and the results of benchmark experimental studies characterizing performance can be found in Donovan et al. [12], He et al. [13], and Donovan [14]. A schematic of the UM-RCF is shown in Fig. 1. Briefly, the UM-RCF consists of five major components: the driver section, the driven section, the test manifold, the sabot (free-piston), and the hydraulic control valve assembly, and in its most basic form can be described as a simple piston-cylinder device. The driver section (154 mm i.d.) acts as a reservoir for high-pressure gases used to operate the UM-RCF and is connected to the driven section by a fast-acting globe valve. The driven section is the cylinder (2.74 m long, 101.2 mm i.d.) through which the sabot travels during operation (the sabot is loaded into the globe valve end of the driven section) and is connected to the test manifold at its other end. Test gases are loaded into the middle of the driven section prior to oper-

ation. During operation, the globe valve is opened (using the hydraulic control valve assembly), permitting the compressed gas to enter the driven section and rapidly accelerate the sabot. The test gas mixture in the driven section is compressed in front of the sabot and sealed within the test manifold. The nosecone of the sabot is not permitted to rebound. For a core region within the test gas mixture, compression is essentially isentropic and the conditions are uniform [12]. Ideally, reactions of interest will occur subsequent to the completion of the compression process.

The test manifold consists of components that permit control of the length of the manifold (extension sections) and that contain the diagnostics available with the UM-RCF (thermocouple manifolds and the test section). Two extension sections were used individually or in series to control the overall compression ratio and gas temperatures. The thermocouple manifolds are designed for the mounting of fine-wire thermocouples (Omega Engineering P10R-001) across the bore of the test manifold and were used to obtain qualitative temperature measurements at various locations, both axially and radially, within the test manifold. The test section is equipped with two optical ports (used with the OH laser absorption diagnostic described below), a pressure transducer port (a Kistler 6041AX4 piezoelectric transducer with a Kistler 5010B charge amplifier were used in the current study), two additional instrumentation ports, and a gas inlet/outlet port. A transparent polycarbonate end wall seals the test manifold.

The sabot is constructed of two parts (Fig. 2), an acetal resin (Delrin) body and an ultrahigh molecular-weight (UHMW) polyethylene replaceable nose cone. Two spring-loaded U-rings seal the sabot in the bore of the test section and prevent blow-by of the pressurized driver gases used to accelerate the sabot. The nose cone is slightly tapered so that it will seal in the extension section of the test manifold with an interference fit.

Fixed-frequency UV absorption spectroscopy, using an argon-ion pumped ring dye laser as the emission source, was used to measure the concentration of

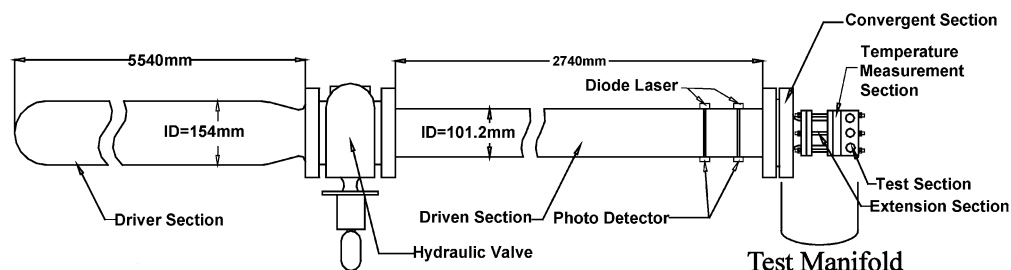


Fig. 1. Schematic of the University of Michigan rapid-compression facility.

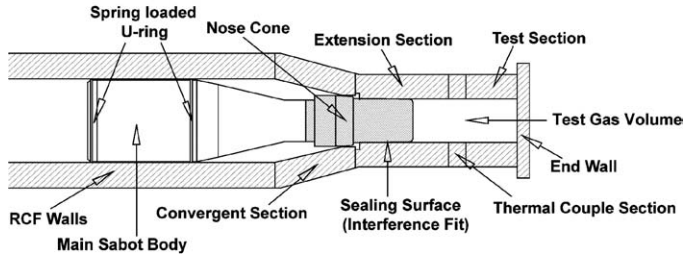


Fig. 2. Photograph and schematic of the sabot used in the UM-RCF and the sealing mechanisms. In the photograph, the black portion is the main body of the sabot and the white portion is the replaceable nose cone. The two U-ring seals can be seen on the main body of the sabot. Note that the sabot seals the test manifold by means of an annular interference fit between the nose cone and the extension section.

OH radicals (χ_{OH}) in the gas mixture. The UV absorption diagnostic is an adaptation of the previously reported frequency-modulated UV diagnostic. Details of the diagnostic can be found in Donovan et al. [15] and Donovan [14]. For these experiments the laser frequency was not modulated, and instead was fixed at the resonant frequency of the $R_1(5)$ transition in the $A^2\Sigma^+ \leftarrow X^2\Pi_i(0, 0)$ band of the OH spectrum, $\nu_0 = 32606.556 \text{ cm}^{-1}$. The wavelength of the UV laser was confirmed using a wavemeter and scanning the $R_1(5)$ transition in a reference flame prior to the commencement of each experimental run.

The silane/oxygen mixtures investigated were highly dilute (SiH_4 mole fractions of 0.5%), lean (nominal equivalence ratio, ϕ , of 0.5), and prepared at subatmospheric pressures (typically 4.6 kPa), and used nitrogen as the primary diluent. Effective compression ratios ranged from 16 to 20. The nominal mixture compositions and compression ratios are summarized in Table 1. Diluent composition and compression ratios were varied to control experimental temperatures and pressures with conditions 1–4 in Table 1 representing increasing temperatures and pressures. Constituent gases had purities of at least 99.998%, except for O_2 , which had a purity of 99.98%.

Multiple strategies for the preparation of stable silane/oxygen/diluent test gas mixtures were investigated and are documented in Donovan [14]. Repeatable preparation of stable mixtures was only achieved by in situ mixing of the components within the cleaned, purged, and evacuated driven section of the UM-RCF (evacuated to $P < 32 \text{ Pa}$). The gases were

Table 1
Experimental conditions

Condition	Nominal mole fraction (%)				Target compression ratio
	SiH_4	O_2	N_2	Ar	
1	0.50	2.0	97.5	0.0	16–17
2	0.50	2.0	97.5	0.0	18–20
3	0.50	2.0	81.5	16.0	18–20
4	0.50	2.0	66.0	31.5	18–20

allowed to mix (by diffusion) for a period of 20 to 50 min before each experiment. The time required for adequate mixing was determined through experimental testing. During the mixing period, some in-leakage of gases occurred (approximately 1.3 Pa/min, resulting in a total in-leakage of less than 1% of the total mixture on a mole basis). For the purposes of calculations of mixture fractions, the composition of in-leakage was assumed to be standard air (dry air composition of 78.11% N_2 , 20.96% O_2 , balance argon) with a relative humidity of 50% at room temperature and atmospheric pressure. Based on this assumed humidity, the resulting H_2O concentration in the test gas mixture is estimated at approximately 270 ppm. The mixtures were monitored for prereaction using a diode laser ($\sim 630 \text{ nm}$) aimed down the length of the driven section. Scattering of the laser emission by silica particles (formed by reaction between the silane and oxygen) is easily noted and is a clear indication of prereaction. Each of the experiments had no indications of prereaction and the experimental data were consistent with the existence of a homogeneous mixture in the test volume. The silane mole

fractions studied were selected based on an upper limit for χ_{SiH_4} set by prereaction and a lower limit set by acceptable signal-to-noise ratios for the χ_{OH} diagnostic.

2.1. Typical experimental results and data analysis

Fig. 3 presents typical experimental data. The upper portion of Fig. 3 shows the pressure and uncorrected temperature time histories. The lower portions of Fig. 3 display output from the reference (I_0) and the transmitted (I) signals from the photodiode detectors used to monitor the differential absorption of the UV laser emission. The calculated difference between the two detector outputs ($\Delta I = I_0 - I$) is also provided. In Fig. 3, the time scale has been chosen such that $t = 0$ denotes the end of the compression process and the maximum recorded pressure.

Several features of Fig. 3 are worth noting, as they are common to all the data. A sudden pressure increase is recorded during the compression at $t \approx -16$ ms. Coincident with the pressure increase, the temperature time history of the center thermocouple (T_c) inflects upward. (Note, the relatively slow time response of the thermocouples, on the order of 10 ms, transforms the expected sudden increase in temperature that accompanies ignition into the observed inflection in the temperature time history.) Less than 1 ms after the first inflection, a similar inflection is seen in the temperature time history measured by the boundary thermocouple (T_b). The sudden pressure increase is an indication of the initial reaction

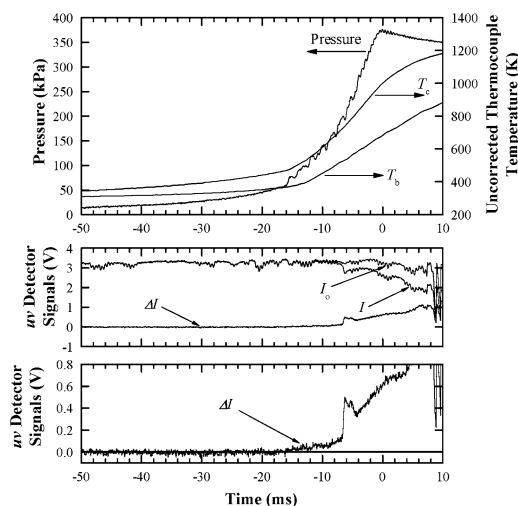


Fig. 3. Typical data from a $\text{SiH}_4/\text{O}_2/\text{inert}$ gas UM-RCF experiment (0.498% SiH_4 , 2.07% O_2 , 15.75% Ar, 270 ppm H_2O , balance N_2 , $P_0 = 4.6$ kPa, and $T_0 = 297$ K). The center (T_c) and boundary (T_b) temperature measurements were recorded at 25.4 and 1.3 mm from the side wall, respectively, where the radius of the test section is 25.4 mm.

between silane and oxygen. The coincident increases in temperature are consistent with this explanation. The slight time difference between the inflections seen in the two temperature time histories is consistent with the reaction propagating rapidly in the radial direction, indicating that chemical kinetics, not fluid mixing, are responsible for reaction propagation. Beyond $t = 0$, the temperature time histories of Fig. 3 are smooth and without any sudden temperature increases. This indicates that no significant chemical reactions are occurring after the compression process is completed.

Note that although it may be preferable for ignition of the test gas mixtures to occur at constant volume conditions (i.e., after the test gases are sealed in the test section, in order to facilitate data analysis and interpretation), experimental constraints (e.g., minimum concentrations required for detectable OH signals) resulted in silane combustion systems which always reacted during compression, as seen in Fig. 3. Due to the well-characterized nature of the compression process [12,14] (i.e., a large, uniform core region which undergoes essentially isentropic compression), analysis of the current experimental results is only slightly more complex than the situation of postcompression reaction.

The pressure increase at $t \approx -16$ ms is followed by a series of pressure oscillations. The fluctuations increase in frequency until peak compression is reached. The pressure oscillations are believed to be pressure waves originating due to the explosive nature of the silane–oxygen reaction. An analysis of this hypothesis was conducted on the experimental data presented in Fig. 3 by evaluating the characteristic frequency of the oscillations and estimating the time for pressure waves to travel the axial distance of the driven section. For the analysis, the following assumptions were made: pressure disturbances travel at the local sonic velocity and the time between peaks (or valleys) in the pressure time history is the time for a pressure wave to travel the distance between the front of the sabot and the end wall of the test section and back. The gas temperature was determined using the chemical kinetics model described below, and the ratio of specific heats was calculated based on a mixture of 84.3% nitrogen and 15.7% argon. The agreement between the measured pressure pulse frequency and the calculated frequency was excellent (e.g., $f_{\text{exp}} = 1290$ Hz and $f_{\text{calc}} = 1282$ Hz).

Another possible explanation for the pressure oscillations is that chemical reaction within the UM-RCF occurs inhomogeneously and develops axially with time. Such behavior could possibly generate the oscillating pressure trends observed in the experimental data. However, inhomogeneous reaction propagation that leads to axial pressure variations would also

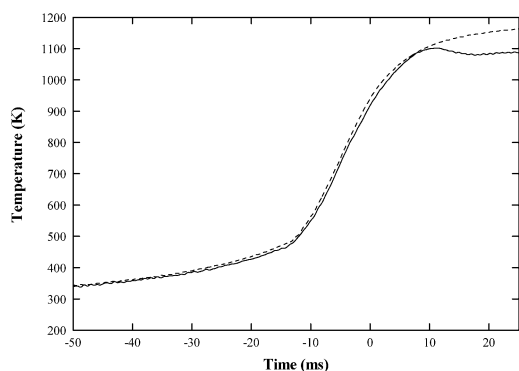


Fig. 4. Uncorrected temperature profiles at two axial locations (solid line = 170 mm from the end wall, dotted line = 64 mm from the end wall) from a $\text{SiH}_4/\text{O}_2/\text{inert}$ gas UM-RCF experiment. Experimental conditions are nominally condition 3 of Table 1.

lead to axial variations in temperature within the test volume. Axial variations in temperature were investigated by installing two thermocouple manifolds separated by an extension section. The axial separation between the two sets of thermocouples was 106 mm. Fig. 4 presents the uncorrected temperature measurements from this investigation. As seen in Fig. 4, the temperature profiles at the two locations are nearly identical throughout the compression process and no indication of the axial development of chemical reactions is observed. Therefore, axial inhomogeneities are not considered a valid explanation for the observed pressure oscillations. Deviations observed approximately 9 ms after compression are due to both bulk fluid motion from the front of the decelerating sabot and vibration of the thermocouples.

The data from the UV fixed-frequency absorption diagnostic (Fig. 3) contain several features of interest. The most important feature is the absorption peak that is observed between $t = -7$ and -4 ms. This feature is only present in experiments with the UV laser tuned to the resonant frequency for the $R_1(5)$ transition. It is absent in experiments conducted with the UV laser tuned to a nonresonant frequency and also in inert gas experiments with the UV laser tuned to the resonant frequency for the $R_1(5)$ transition. These observations confirm that this absorption peak is due to the presence of OH within the test section.

The gradual increase in ΔI , which is observed starting shortly after the pressure disturbance noted previously and continues until, and somewhat beyond, the point of peak compression ($t = 0$), is attributed primarily to scattering by small silica particles formed as products of the silane/oxygen combustion. The same behavior in ΔI is seen when the UV laser is tuned to a nonresonant frequency, but it is not observed in inert gas experiments. Attributing this

effect to particle scattering is also supported by an estimate of the particle loadings of 10^{12} particles/ cm^3 (corresponding to a particle volume fraction of 4 ppm, based on full conversion of the silane to silica and assuming 20-nm-diameter particles) and the presence of fine particles on the optical windows at the conclusion of the experiment.

A secondary cause of the increase in ΔI is due in part to deflection of the signal beam caused by strain on the sapphire optical windows as the pressure (and temperature) increases in the test section. While the windows are designed to minimize beam deflection due to strain (the optical axis of the windows is perpendicular to the face of the windows), if the signal beam is not aligned perpendicular to both windows, deflection can occur. This deflection causes the UV laser beam to gradually drift off the active element of the detector as the pressure (and temperature) increases. Consequently, drift manifests itself as a gradual decrease in I (thus increasing ΔI). Particular care was taken to ensure good optical alignment of the UV laser beam for all data presented in this study; however, the effects of beam deflection are observed in some experiments. Both nonresonant absorption and beam drift were accounted for in the postprocessing of the UV absorption data. A detailed discussion of the correction procedures can be found in Ref. [14].

The transmission ratio I/I_0 was calculated using the techniques outlined in Refs. [14,15] and χ_{OH} was determined from I/I_0 using Beer's law. Due to the lack of quantitative experimental temperature measurements the temperatures determined by the computational modeling (described below) were used in the determination of χ_{OH} . (Correcting for the time response of the thermocouples in the presence of chemical reactions results in large experimental uncertainties and therefore was not performed for this work.) Based on the level of agreement between the experimental and the calculated pressure time histories, the accuracy of using the modeled temperature is estimated at $\pm 10\%$.

2.2. Uncertainty analysis

Several uncertainties in experimental conditions contribute to uncertainty in the determination of χ_{OH} . A summary of the uncertainties and the effects on χ_{OH} are presented in Table 2. Combining the sources of uncertainty yields an overall uncertainty in χ_{OH} of 32/–29%. Based on the noise levels observed experimentally ($\sim 2\%$ of the reference signal strength), temperatures and pressures typical of the experimental data presented herein, and the uncertainties calculated above, the detection limit of the diagnostic is estimated at 15 ppm.

Table 2
Experimental uncertainties

Uncertainty source	Direct uncertainty	U_i = Uncertainty in χ_{OH}
Nonresonant absorption	$\pm 20\%$ in absorption	$\pm 23\%$
Laser source departure from resonant frequency	$\pm 0.05 \text{ cm}^{-1}$ in laser frequency	+15%
Temperature estimation	$\pm 10\%$ in temperature	$\pm 13\%$
Pressure oscillations	$\pm 5\%$ in pressure	$\pm 3.2\%$
Transducer linearity and amplifier drift	$\pm 5.02 \text{ kPa}$	$\pm 2.3\%$
Temperature uniformity	$\pm 5\%$ in temperature	$\pm 5\%$
Path length	$\pm 1.0 \text{ mm}$ in path length	5.6/–8.0%
Spectroscopic parameters	Various	$\pm 5\%$

Note. Combined uncertainty ($\sqrt{(\sum U_i^2)}$) = 32/–29%.

2.3. Computational modeling

To aid in the interpretation of the χ_{OH} profiles obtained from the UM-RCF experiments, the Aurora/Chemkin 3.7.1 library [16] was used to model the compression process and chemical reaction within the UM-RCF. The combustion model was a spatially uniform mixture with time varying composition (due to chemical reaction) and volume (due to compression). The gas volume as a function of time was determined using nonreacting experiments and scaled to the specifics of the reacting gas experiments based on the measurement of sabot position at three locations within the driven section of the UM-RCF. A modified version of the chemical kinetics mechanism proposed by Kondo et al. [17] was used for the Aurora simulations. The modifications included addition of the clustering reactions of Suh et al. [8] and modifications to the H_2/O_2 chemistry. The reaction mechanism used is provided in Ref. [18]. Further details of the computational modeling conducted are provided in Ref. [14] and the Aurora input files are provided in Refs. [14,18]. Additional mechanisms proposed by Britten et al. [19], Babushok et al. [20], and Miller et al. [21] were initially evaluated in this study. While these mechanisms are each effective at predicting silane combustion phenomenon under the varied ranges of experimental conditions for which they were developed, they failed to reproduce the key experimental features observed in the current study. Specifically, the modified Kondo mechanism predicted two-stage ignition, whereas the other three mechanisms failed to predict two-stage ignition and generally did not reproduce either the ignition temperature, ignition rate, or the observed OH concentration. Consequently, these mechanisms were not considered further in this work.

In addition to a chemical kinetics mechanism, other inputs required by Aurora are the initial conditions (pressure, temperature, and mixture composition), and a description of the compression process within the UM-RCF. The initial pressure and tem-

perature are recorded at the start of each experiment and the determination of mixture composition was discussed previously. Modeling of the UM-RCF compression process within Aurora is discussed below.

The Aurora/Chemkin library is designed as a tool to model the transient properties of a well-mixed reactor. The UM-RCF is just such a reactor. Using Aurora to model the compression process within the UM-RCF requires a relationship for the test volume as a function of time. Earlier characterization studies of the UM-RCF [12,14] have demonstrated that isentropic relations can be used to accurately model the compression of a core region of the test volume. Unfortunately, due to the chemical reaction that occurs during compression, these isentropic relationships can only be applied up to the point of reaction and cannot be used to derive a relationship for the entire volume time history from the experimental pressure time history. In the absence of isentropic relations describing the entire compression process, UM-RCF experiments with inert gases were used as surrogates to calculate the volume as a function of time. These inert gas experiments were conducted under similar conditions (hardware configuration, initial pressures, gas concentrations, sabot velocities, and compression ratios) to the reactive mixture UM-RCF experiments. Since no chemical reactions occur in these experiments, isentropic relationships can be used to calculate the entire volume time history from the pressure time history. Further details of this modeling process are provided in Ref. [14].

3. Results

Figs. 5–8 present experimental and modeling results from four representative silane/oxygen experiments with experimental conditions 1–4 of Table 1. In each figure, the time scale has been chosen such that $t = 0$ denotes the end of the compression process and the maximum recorded pressure.

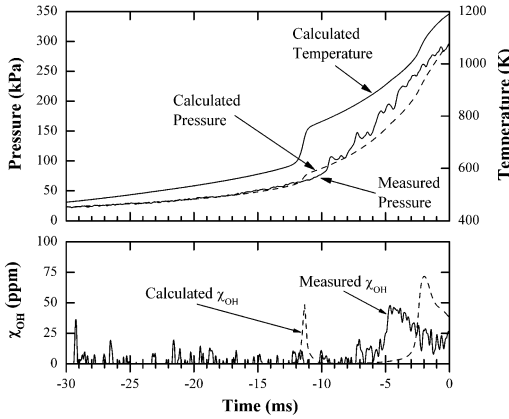


Fig. 5. Experimental and modeling results for: $T_0 = 296$ K, $P_0 = 4.6$ kPa, 97.40% N_2 , 2.07% O_2 , 0.50% SiH_4 , 260 ppm H_2O , and 150 ppm Ar, $\phi = 0.48$ —condition 1.

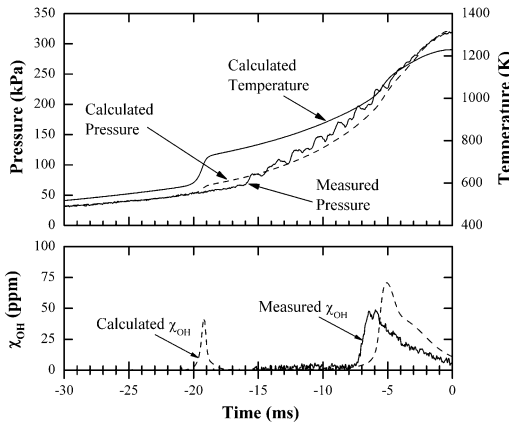


Fig. 6. Experimental and modeling results for: $T_0 = 298$ K, $P_0 = 4.6$ kPa, 97.39% N_2 , 2.07% O_2 , 0.50% SiH_4 , 290 ppm H_2O , and 170 ppm Ar, $\phi = 0.48$ —condition 2.

Figs. 5–8 each consist of two graphs. The upper graph is a plot of the measured pressure and the calculated temperature and pressure, as determined by the computational modeling. The lower graph depicts the measured and calculated OH mole fractions. As stated earlier, the temperature used to determine χ_{OH} was taken from the results of the computational model.

Several trends are evident in Figs. 5–8. In all of the experimental data, a sudden pressure rise is observed 9 to 21 ms before the end of compression. The pressure rise is accompanied by an abrupt upward inflection (see earlier discussion in Section 3) in the slope of the uncorrected thermocouple data (not shown in Figs. 5–8). The pressure rise identifies ignition of the silane/oxygen mixture. Pressure oscillations follow ignition and, as discussed previously, are due to the pressure waves generated by the extremely rapid reaction between silane and oxygen.

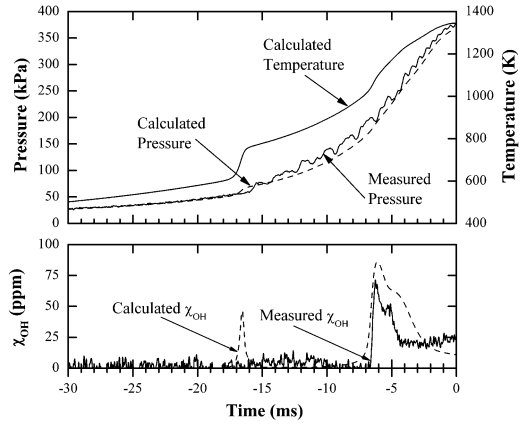


Fig. 7. Experimental and modeling results for: $T_0 = 297$ K, $P_0 = 4.6$ kPa, 81.66% N_2 , 15.75% Ar, 2.07% O_2 , 0.50% SiH_4 , and 270 ppm H_2O , $\phi = 0.48$ —condition 3.

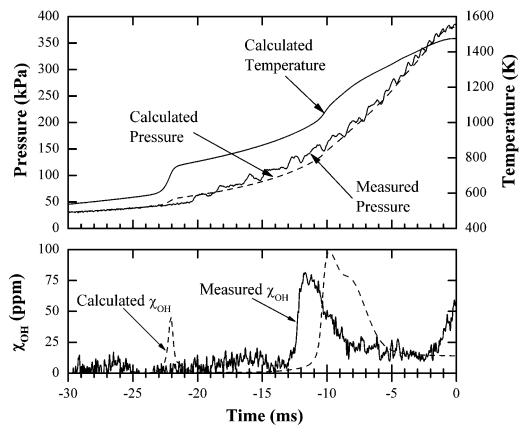


Fig. 8. Experimental and modeling results: $T_0 = 298$ K, $P_0 = 4.6$ kPa, 65.93% N_2 , 31.46% Ar, 2.08% O_2 , 0.50% SiH_4 , and 290 ppm H_2O , $\phi = 0.48$ —condition 4.

Consistent with the experimental data, the computational model predicts similar changes in pressure, though these changes occur 2 to 4 ms earlier than observed experimentally. The model confirms that the pressure rise is the result of ignition of the silane/oxygen mixture. As all properties are treated as spatially uniform within Aurora, the model is unable to reproduce the pressure oscillations observed in the experimental data. Agreement between the measured and calculated pressures is excellent up to the start of combustion, and agreement is generally good from that point until the end of compression.

The experimental data show a single absorption feature from the UV absorption diagnostic at 4 to 9 ms after the start of combustion. The magnitude of the peak absorption is from 8 to 12% and corresponds to χ_{OH} of 47 to 82 ppm. As can be seen by comparing the data of Figs. 5–8, the peak OH concentration in-

creases as temperature increases. Absorption due to beam scattering and nonresonant absorption is evident in each set of experimental data and begins approximately 2 ms after ignition occurs. As discussed above, the appearance of nonresonant absorption is an indication of the formation of particles and establishes the delay between chemical ignition and (detectable) particle formation at less than 2 ms.

Unlike the experimental data, the kinetics model predicts two peaks in χ_{OH} ; a smaller peak at the start of combustion and a second larger peak 9 to 14 ms later. While no OH is measured experimentally at the time of this first predicted peak in χ_{OH} , this first peak does coincide with the experimental pressure rise noted previously, and is a further (computational) indication of ignition of the silane/oxygen mixture. The second predicted peak in χ_{OH} coincides with the experimentally measured χ_{OH} , though the predicted peak χ_{OH} tends to occur later and is 25 to 50% higher than the measured peak χ_{OH} .

4. Discussion

The experimental and computational results are summarized in Table 3. The summary includes data from Figs. 5–8 as well as data from additional experiments both with and without the UV absorption diagnostic. The ignition temperatures in Table 3 were calculated from the pressure time histories using isentropic relations. Here, ignition is defined based on the appearance of significant radical concentrations (i.e., chemical ignition) and not the observed increase in pressure. The rationale for this definition of ignition is discussed below. As seen in Table 3 (where the temperature ranges represent the limits of the observed ignition temperature for each condition), the calculated ignition temperatures are essentially uniform for all experimental conditions studied: 629 ± 17 K. The computational models predict a somewhat lower, though similarly uniform, ignition temperature of 593 ± 12 K.

Table 3
Summary of experimental and computational results

Condition	Ignition temperature (K)		Maximum χ_{OH} (ppm)		Experimental P_{max} (kPa)
	Exp. ^a	Calc.	Exp.	Calc.	
1	627–645	605	47.7	71.7	295
2	623–626	581–582	44.7–48.7	68.2–70.8	303–320
3	619–623	599	71.3	86	376
4	612–626	586–598	80.7–81.6	98.1–98.4	385–387
Avg.	629 ± 17	593 ± 12			

^a Experimental temperatures are calculated from the measured pressure at the time of ignition and the initial pressure and temperature using isentropic relations.

Because combustion occurs during the compression process, the observed pressure rise may not be a good indicator of the start of ignition. Fig. 9 presents predicted key species (SiH_4 , O_2 , H_2 , and OH) concentrations and temperature and pressure profiles for the experimental conditions presented in Fig. 7. As can be seen in Fig. 9, key radicals, such as OH , are predicted to appear more than 1 ms prior to the pressure and temperature increases and SiH_4 decomposition (and subsequent H_2 formation) starts even earlier. During this delay between chemical ignition and heat release (observed as the rapid increase in pressure and temperature), the test gas mixture continues to be compressed and thus heated. The amount of compression heating that occurs during this short time period is directly dependent on the specific heat ratio of the gas mixture; mixtures with higher concentrations of Ar have higher specific heat ratios and therefore experience greater heating than mixtures with less argon. This dependence of compression heating on gas composition causes mixtures with greater argon concentrations to have higher temperatures at the time of the observed pressure rise. Thus, the pressure rise is convolved with the compression heating, making pressure a poor indicator of ignition temperature.

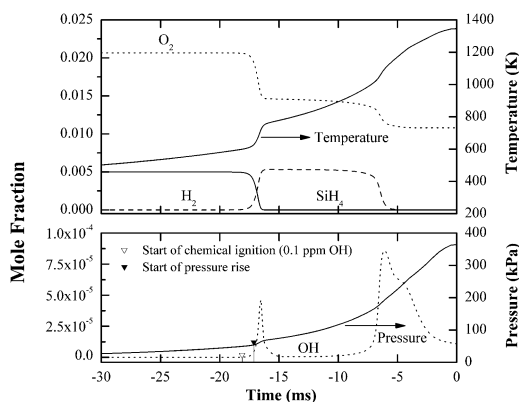


Fig. 9. Primary fuel and oxidizer species concentrations from the kinetics modeling of the experimental data of Fig. 7.

To minimize the influence of compression heating on the determination of the ignition temperature, the following methodology was used to define ignition. For the computational modeling, chemical ignition was defined to occur when χ_{OH} exceeded 0.1 ppm. This benchmark was typically reached approximately 1 ms prior to the predicted pressure rise. As no OH was experimentally detected at ignition the experimental χ_{OH} could not be used to directly define the point of ignition. Instead, the experimental ignition point was defined to occur 1 ms prior to the observed increase in pressure, consistent with the computational predictions.

A key result from the kinetics modeling is the prediction that silane combustion occurs in two stages. As can be seen in Fig. 9, the first stage is the complete reaction of silane with oxygen and the second stage is the reaction of molecular hydrogen (formed during the combustion of the silane) with the remaining oxygen. This two-stage combustion behavior was predicted by Babushok et al. [20] for low silane concentrations, but has not been observed prior to these experiments. The production of molecular hydrogen from the initial reaction between silane and oxygen is consistent with the earlier experimental observations of Tokuhashi et al. [22], who noted significant hydrogen concentrations in the products of their lean SiH_4/O_2 flames. The two-stage reaction predicted by the kinetics model is in excellent agreement with the experimental data, except for the presence of OH during the first stage. The pressure rise, which accompanies the heat release during the first stage, is clearly seen in both the experimental data and the modeling results. The experimentally measured OH coincides with the location of the second stage of the combustion predicted by the model.

As seen in Figs. 5–8, experiments with higher peak pressures, and by inference higher peak temperatures, have higher measured χ_{OH} . As the kinetic modeling shows, the detected OH is a result of hydrogen–oxygen combustion, where hydrogen is produced as a by-product of the combustion of silane. Since lower temperatures favor the removal of OH in hydrogen/oxygen combustion, lower mole fractions of OH are both expected and observed in experiments with lower temperatures (see also Table 3).

As noted, the kinetics modeling predicts the production of a significant quantity of OH at ignition. The predicted χ_{OH} is within the detection limit of the UV absorption diagnostic, yet no OH is observed at this point. While several experimental explanations for this discrepancy come to mind (e.g., inhomogeneous reactions, OH lifetimes which are too short to detect, and excessive estimation of the optical path length), none of these explanations survives scrutiny. Inhomogeneous reactions are not supported by radial

thermocouple measurements, which record ignition within a fraction of a millisecond of each other—far too fast to explain the failure to detect the presence of OH. Unless the removal of OH is more rapid than predicted by the kinetics model, the time response of the UV absorption diagnostic (less than 12.3 μs) is more than sufficient to detect the predicted OH concentrations. The estimates for path length are conservative (determined by radial thermocouple measurements to be 70% of the test section diameter [12]), and the change necessary to decrease the predicted OH concentrations to below detectable levels is more than a factor of two.

A key reaction which affects the OH concentration during silane combustion is $\text{SiH}_3 + \text{O}_2$. This reaction has several parallel, and competing, product paths that lead to the production of H, O, and OH, respectively. The absence of OH at ignition of silane/oxygen mixtures suggests that OH is not a significant radical in early silane combustion; the OH-branching fraction of the $\text{SiH}_3 + \text{O}_2$ reaction may not have been properly considered in the Kondo mechanism [17]; and this branching fraction may be much lower than previously reported [23–25].

With the mechanism of Kondo et al. [17] the ignition of silane can be very sensitive to H_2O concentration. Since the water concentration used in the kinetic modeling is based on an estimate of relative humidity, a study of the sensitivity of silane ignition to the assumed relative humidity was undertaken. In summary, a 20% change in relative humidity (from 50 to 40%) results in a 7 and 2% increase in peak χ_{OH} and a 1.2- and 0.2-ms delay in appearance of the peak at the first and second stages of combustion, respectively. The H_2O concentration has a much larger effect at lower concentrations, and an evaluation of these effects is provided in Ref. [14].

5. Conclusions

The current work presents the first absolute, quantitative measurements of χ_{OH} and the first documented observation of two-stage ignition in a silane combustion system. Several key features of silane combustion have been identified. Silane combustion is observed to occur in two distinct stages, separated in time by greater than 5 ms. While theorized, experimental observation of two-stage combustion of silane has not been previously reported, most likely due to the long test times and lower temperatures required to observe this phenomenon. Based on kinetics modeling, the first stage is the reaction of silane with oxygen and the subsequent production of molecular hydrogen. The first stage is easily identified by a sudden rise in experimental and predicted pressure and

temperature. Although the kinetics model predicts the formation of OH during the first stage of combustion, this is not observed experimentally. The second stage of combustion is the subsequent reaction of hydrogen with the remaining oxygen. The second stage is identified by significant production of OH ($\chi_{\text{OH}} = 45\text{--}82$ ppm).

Experiments were performed with several mixtures, varying the dilution and heat capacity in order to change the rate of compression heating. These changes had minimal impact on ignition, which was observed to occur at 629 ± 17 K for all experiments presented herein. The consistency of ignition temperature was replicated with the kinetics modeling.

As stated above, the chemical mechanism predicts the formation of a significant quantity of OH during the first stage of silane combustion. No OH was detected in the experiments during the first stage of reaction. The detection limit of the OH absorption diagnostic sets an upper limit on the amount of OH present during the first stage of ignition (χ_{OH} must be less than 15 ppm). The absence of OH at the ignition of silane/oxygen mixtures suggests that OH is not a significant radical early in the silane combustion process and that the OH-branching fraction of the $\text{SiH}_3 + \text{O}_2$ reaction is lower than previously reported [23–25]. Current work includes detailed investigation of this reaction and the development of an improved silane mechanism that can reproduce the two-stage ignition features observed in this work.

Particle formation, as detected by nonresonant absorption of the UV laser emission, is observed approximately 2–5 ms after ignition of the silane/oxygen mixture and prior to the second stage of combustion. The delay between ignition and particle accumulation is an indication of the rapidity of the particle nucleation and growth processes in silane systems. While this work only estimates particle loading based on coarse scattering calculations, additional investigations are planned to further bridge the gap between gas-phase chemistry and the early stages of nanoparticle nucleation.

Acknowledgments

The authors acknowledge the generous support of the National Science Foundation and the Department of Energy and thank Professor Alec Gallimore for his assistance with the laser frequency measurements.

References

- [1] M.R. Zachariah, D. Chin, H.G. Semerjian, J.L. Katz, *Combust. Flame* 78 (1989) 287–298.
- [2] M.R. Zachariah, H.G. Semerjian, *AIChE J.* 35 (1989) 2003–2012.
- [3] M.S. Wooldridge, P.V. Torek, M.T. Donovan, D.L. Hall, T.A. Miller, T.R. Palmer, C.R. Schrock, *Combust. Flame* 131 (2002) 98–109.
- [4] A.G. McLain, C.J. Jachimowski, R.C. Rogers, NASA Technical Paper 2114, 1983.
- [5] C.J. Jachimowski, A.G. McLain, NASA Technical Paper 2129, 1983.
- [6] M.A. Ring, H.E. O’Neal, J. Famil-Ghiriha, in: W. Luft (Ed.), *AIP Conference Proceedings: Photovoltaic Safety*, American Institute of Physics, New York, 1988, pp. 175–182.
- [7] S.L. Girshick, M.T. Swihart, S.-M. Suh, M.R. Mahajan, S. Nijhawan, *J. Electrochem. Soc.* 147 (6) (2000) 2303–2311.
- [8] S.-M. Suh, M.R. Zachariah, S.L. Girshick, *J. Vac. Sci. Technol. A* 19 (3) (2001) 940–951.
- [9] E.L. Peterson, M.W. Crofton, *AIAA Conference Paper* 2002–3875, 2002.
- [10] J.R. Hartman, J. Famil-Ghiriha, M.A. Ring, H.E. O’Neal, *Combust. Flame* 68 (1987) 43–56.
- [11] S. Kondo, K. Tokuhashi, H. Nagai, M. Iwasaka, M. Kaise, *Combust. Flame* 97 (1994) 296–300.
- [12] M.T. Donovan, X. He, B.T. Zigler, T.R. Palmer, M.S. Wooldridge, A. Atreya, *Combust. Flame* 137 (3) (2004) 351–365.
- [13] X. He, M.T. Donovan, T.R. Palmer, B.T. Zigler, M.S. Wooldridge, A. Atreya, in: *Proceedings of the Third Joint Meeting of the U.S. Sections of The Combustion Institute*, March 16–19, 2003, pp. 1–6, paper B24; X. He, M.T. Donovan, B.T. Zigler, S. Walton, T.R. Palmer, M.S. Wooldridge, A. Atreya, in: *Proceedings of the 2003 Technical Meeting of the Eastern States Section of the Combustion Institute*, October 26–29, 2003, pp. 209–212, paper 53.
- [14] M.T. Donovan, Ph.D. thesis, University of Michigan, Ann Arbor, MI, 2003.
- [15] M.T. Donovan, D.L. Hall, P.V. Torek, C.R. Schrock, M.S. Wooldridge, *Proc. Combust. Inst.* 29 (2002) 2635–2643.
- [16] R.J. Kee, F.M. Rupley, J.A. Miller, M.E. Coltrin, J.F. Grac, E. Meeks, H.K. Moffat, A.E. Lutz, G. Dixon-Lewis, M.D. Smooke, J. Warnatz, G.H. Evans, R.S. Larson, R.E. Mitchell, L.R. Petzold, W.C. Reynolds, M. Caracotsios, W.E. Stewart, P. Glarborg, C. Wang, O. Adigun, W.G. Houf, C.P. Chou, S.F. Miller, *Chemkin Collection*, Release 3.7.1, Reaction Design, San Diego, CA, 2003.
- [17] S. Kondo, K. Tokuhashi, A. Takahashi, M. Kaise, *Combust. Sci. Technol.* 159 (2000) 391–406.
- [18] *Si/H₂/O₂ Mechanism*, Version 2.0, 2/28/2004, University of Michigan, Ann Arbor, MI, 2003, available at: www.personal.engin.umich.edu/~mswool/.
- [19] J.A. Britten, J. Tong, C.H. Westbrook, *Proc. Combust. Inst.* 23 (1990) 195–202.
- [20] V.I. Babushok, W. Tsang, D.R. Burgess, M.R. Zachariah, *Proc. Combust. Inst.* 27 (1998) 2431–2439.
- [21] T.A. Miller, M.S. Wooldridge, J.W. Bozzelli, *Combust. Flame* 137 (1–2) (2003) 73–92.

- [22] K. Tokuhashi, S. Horiguchi, Y. Urano, M. Iwasaka, H. Ohtani, S. Kondo, *Combust. Flame* 82 (1990) 40–50.
- [23] M. Koshi, N. Nishida, Y. Murakami, H. Matsui, *J. Phys. Chem.* 97 (1993) 4473–4478.
- [24] C.L. Darling, H.B. Schlegel, *J. Phys. Chem.* 98 (1994) 8910–8913.
- [25] Y. Murakami, M. Koshi, H. Matsui, K. Kamiya, H. Umeyama, *J. Phys. Chem.* 100 (1996) 17,501–17,506.